J. Condensed Matter Nucl. Sci. 33 (2020) 145–167

Research Article

Elliptic Tracks: Evidence For Superluminal Electrons?

Keith A. Fredericks*

Restframe Labs, 310 W. 52nd St., New York, NY 10019, USA

Abstract

In the literature of Low-Energy Nuclear Reactions (LENR), particle tracks in photographic emulsions (and other materials) associated with certain electrical discharges have been reported. Some Russian and French researchers have considered these particles to be magnetic monopoles. The mechanisms of energy deposition and track formation, while among the most important properties, are contradictory and the least understood of all of the observations. Our method of producing these tracks differs markedly from most other studies in that no electrical discharge is used as a source. Rather, tracks are created with a simple uniform exposure to photons. This simpler method of producing exactly the same tracks supports a more comprehensive exploration of particle track properties. Out of 750 exposures with this method, *elliptic particle tracks* were detected, 22 of which were compared to Bohr–Sommerfeld electron orbits in an idealized model. Ellipses fitted to the tracks were found to have quantized semi-major axis sizes with ratios of $\simeq n^2/\alpha^2$ to corresponding Bohr–Sommerfeld hydrogen ellipses. This prompts inquiry relevant to magnetic monopoles due to the n^2/α^2 force difference between magnetic charge and electric charge using the Schwinger quantization condition. Analogy with the electron indicates that the elliptic tracks could be created by a bound magnetically charged particle with mass $m_m = 1.45 \times 10^{-3}$ eV/c^2, yet with superluminal velocities. Using a modified extended relativity model, m_m becomes the relativistic mass of a *superluminal* electron, with $m_0 = 5.11 \times 10^5$ eV/c^2, the fine structure constant becomes a mass ratio and charge quantization is the result of two states of the electron. Relevance of this new model is considered in light of the observed inconsistencies in track formation.
© 2020 ISCMNS. All rights reserved. ISSN 2227-3123

Keywords: Elliptic orbits, Faster-than-light, Kepler orbits, LENR, Monopoles, Particle tracks, Photographic emulsion, Strange radiation, Superluminal, Tachyons

1. Introduction

In this paper evidence is reported for quantized elliptic tracks in photographic emulsions with sizes expected of bound magnetic monopoles, yet *requiring* velocities greater than the speed of light, indicating particles with superluminal electric charge.

Preliminary measurement of the first recognized elliptic track detection showed a size difference, to within a few percent of $137^2 n^2 \simeq n^2/\alpha^2$ *larger* than an $n = 7$ Bohr–Sommerfeld hydrogen electron orbit, α^{-2} being the difference

*E-mail: keith@restframe.com.

© 2020 ISCMNS. All rights reserved. ISSN 2227-3123

in force between electrons and magnetic monopoles using Schwinger quantization, i.e. Eq. (2). This runs contrary to current expectations suggesting magnetic monopole bound states with *smaller* (*e.g.* 7.2×10^{-18} m) orbit sizes [1] than bound electrons in hydrogen.

Additional experiments provided a collection of elliptic track candidates that were fitted to ellipses. The resulting track fits were quantized according to semi-major axis size, (see Fig. 1) and therefore energy, (see Section 5.3) according to $E^{(n)} = h\nu^{(n)}$, indicating a new particle exhibiting properties of magnetic monopoles. Analogy with the electron and orbit sizes suggest faster-than-light velocities.

Analysis of the results leads to a new model of extended relativity restricted to bound states using a scale transformation rather than the usual superluminal Lorentz transformation (SLT), resulting in the fine structure constant as a mass ratio and a new proposed explanation for charge quantization.

2. Elliptic Tracks

In earlier work [2], properties of new and unusual tracks in photographic emulsions were analyzed and classified. The source of the tracks was unidentified. Analysis showed track configurations clearly distinct from those observed before in nuclear track studies [3], but directly corresponding to tracks from certain studies including:

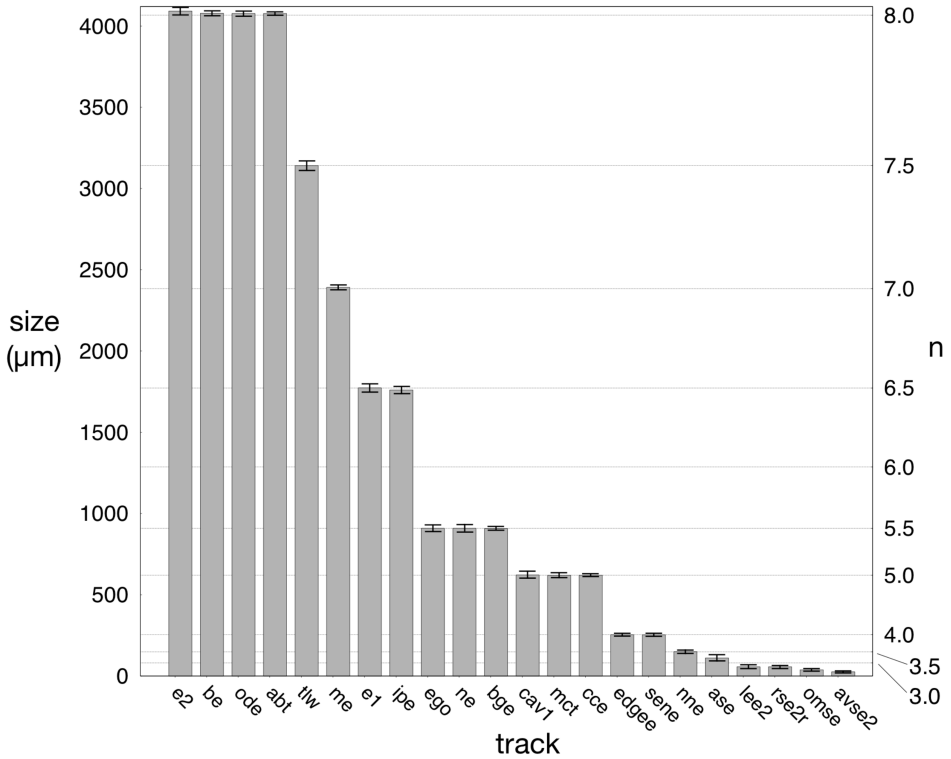

Figure 1. Quantized ellipse semi-major axis sizes. Ellipses between $n = 8$ and $n = 3.5$ are shown to be quantized as half integer values. Ellipses less than $n = 3.5$ are quantized by quarter integer values. Error bars represent the combined standard uncertainty of the semi-major axis size.

(1) exposure of emulsions during bombardment by low-energy ions in electric explosion of metallic wires and thin foils [4–7],
(2) exposure of emulsions during low-energy discharges in water and excitation of beta-decay products by a magnetic field [8],
(3) exposure of emulsions and Pd electrodes during glow discharge plasma processes [9],
(4) exposure of special semiconductor layers during the super-compression of solid targets using electron beams [10], and,
(5) exposures of photographic emulsions, CR-39 (with and without etching), PMMA, and glass during picosecond laser irradiation of electrodes [11].

Ivoilov [8] called this unknown source a *control background*.

Using a simple brief uniform amplifying exposure of photons on photographic emulsions exposed to the environment (as in e.g. a cosmic ray study) duplicates virtually all of the track types presented in the list of studies above. This technique is called photon amplification.

The advantages of photon amplification are:

(1) Tracks can be readily seen in the plastic layer as well as the emulsion layer of photographic films.
(2) Compared to electric discharge sources, simple conditions of the exposure to light bypasses the need for elaborate laboratory setups and hence more data can be gathered (hundreds of exposures) and the phenomenon can be studied more deeply.
(3) Amplification or sensitization of the photographic emulsion due to the uniform photon exposure increases the sensitivity of the photographic emulsion to photons and charged particles.
(4) Detector sensitivity is *re-zeroed* at a higher level by the uniform photon exposure so as to react to tearing down as well as building up of latent image. *White tracks* are detected as well as black tracks.
(5) The light sensitive volume element of the photographic emulsion registers track images of usual time-like particles, which travel through space and, (if they were to exist and are detectable), space-like particles, which would travel through time, since the detector is continually active until the time of development.

This study is concerned primarily with tracks, in photographic emulsions coated on a plastic base, produced during (or after) brief exposures to light. These exposures to light produce a uniform background density on development. Tracks in emulsion are registered against this background density in addition to tracks registered in the plastic base.

Supplemental uniform exposures of photons followed by or combined with imagewise fluxes of particles (traditionally photons) can enhance the sensitivity of photographic emulsions [12]. Giving the supplemental exposure prior to the imagewise exposure is called pre-exposure [13] or pre-flashing. Giving the supplemental exposure during the same time interval is called *concurrent photon amplification* [14]. These techniques were used experimentally by photographic scientists and practically in astronomy and in autoradiography, but (outside of the present study) apparently never used with emulsions for detection of charged particle tracks (nuclear track studies). One of the critical questions to be answered is how is it possible that a particle, responsible for these tracks, has so far evaded detection, especially with a history of perhaps 150 years of the scientific use of photographic emulsions. Here are some possible explanations:

(1) Since the tracks are generally microscopic effects, they would not normally be recognized in non-uniform (standard pictorial photography) backgrounds and, if seen, they would be easy to dismiss or ignore as a processing errors, light leaks or other artifacts.
(2) Since (apparently) no nuclear track studies, that is where emulsions were scanned by greater than $\sim 250x$ magnification, used supplementary photon exposures as amplification, the probability of these new types of tracks remaining unrecognized would be increased.

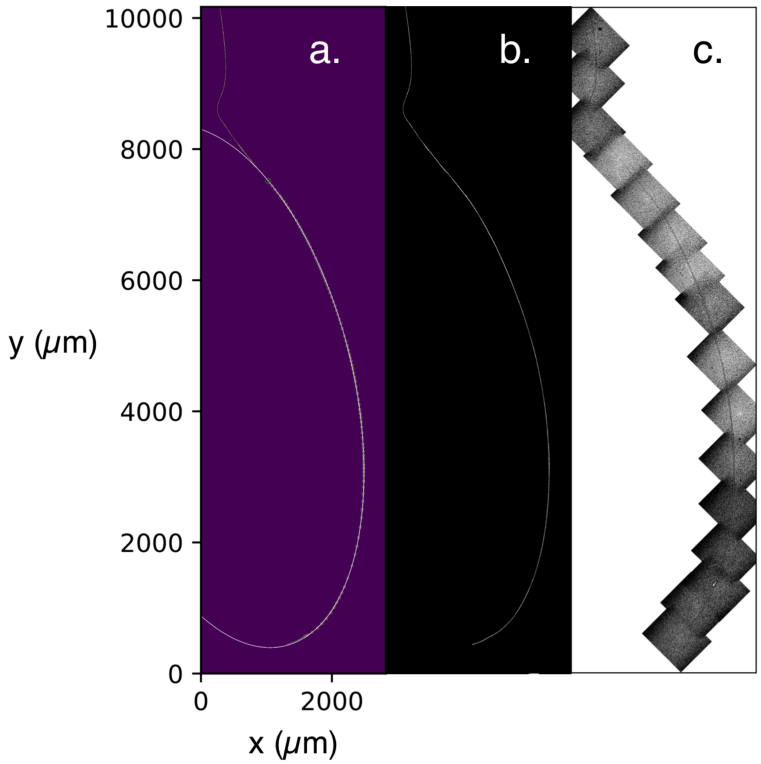

Figure 2. Track *be* (see also Table 1). The semi-major axis size of $a_m = 4078.6 \pm 14.6 \mu m$ is related to the semi-major axis size of an $n = 8$ electron in hydrogen, a_e by $a_m/137^2 n^2 \simeq a_e$. a.) Least-squares fit of x, y track coordinates to ellipse overlayed on processed track image. b.) Track after image processing and background eradication. c.) Photo montage of track.

(3) In the case where no supplemental photon exposure is required to create a baseline background of clear tracks (in plastic base or gelatin), and where magnification greater than $\sim 250\times$ was used to scan emulsions, these tracks may well have not been the object of the search or not of interest, being clear rather than black, or they may have been mistaken for something else like surface damage (cf. [7]).
(4) In the case where no supplemental photon exposure is used and where black tracks, as were reported here, were registered on the film and the film was scanned with greater than $\sim 250\times$ magnification, then it is possible that these tracks were treated as unidentified and never looked at in a deeper way.
(5) In general, the rate of detection/recognition and the flux (see Section 3.7) was reduced and more capricious compared to objects being studied, decreasing the chance of recognition.

For electrically (magnetically) charged particles, it is expected that magnetic fields (electric fields) applied perpendicularly to the plane of particle motion will produce helical curvature and it is expected that electric fields (magnetic fields) applied transversely to the plane of particle motion will produce parabolic curvature. In [2] the possibility of parabolic curvature in magnetic fields for these tracks was incorrectly asserted. In a large number of experiments using applied magnetic fields from $\sim 6.0 \times 10^{-4}$ to ~ 0.7 T, and electric fields from $\sim 1 \times 10^5$ to 2×10^5 V/m, these particles have not, so far, appeared to follow helical or parabolic paths. Rather, they appear to move in other unpredictable ways.

During these experiments, however, repeatable evidence has been found for tracks with elliptic curvature occurring in the presence *or absence* of applied electric and/or magnetic fields (see Figs. 2–7 and 10). Detection of elliptic curvature is probably the most significant breakthrough in the study of these tracks, providing the possibility to compute, under certain assumptions, via *purely geometrical considerations*, properties of particles capable of creating these tracks.

3. Experimental

3.1. Technique

Experiments between May 2014 and December 2017 used uniform photon amplification of films with applied magnetic and electric fields in various configurations. Results were scanned for curved tracks.

Film types Arista Ortho Litho 3.0 or Rollei Ortho 25 were exposed both in 10.2 cm $\times$ 12.7 cm and 3 cm $\times$ 12.7 cm sheets. LED and applied electric and magnetic field exposures were controlled using an Arduino Uno.

3.2. LED exposure

Two or four white LEDs at a 3–6 cm distance from the film plane were turned on simultaneously for a 50–2000 ms exposure. Various white LED lamps were used for the uniform amplifying exposure. These LEDs have a typical luminous intensity of 1250 $\pm$ 15% mcd.

3.3. Applied fields

Abbreviations in boldface appear in the legend of Table 1.

- **DM** Permanent magnet.
  - N45 NdFeB Disc magnet,
  - flux density = 1.32 T,
  - radius = 9 mm,
  - height = 3 mm.
- **BM** Permanent magnet.
  - N40 NdFeB block magnet,
  - flux density = 1.26 T,
  - 50 mm $\times$ 50 mm $\times$ 20 mm.
- **YM** Permanent magnet
  - N42 NdFeB Yoked magnet,
  - flux density = 0.5 T (center line between poles perpendicular to the x,y plane of the film),
  - 100 mm $\times$ 6 mm $\times$ 9 mm.
- **AH** Anti-Helmholtz Coil.
  - number of turns = 10,
  - current per coil = 3.0 A,
  - coil radius = 12.7 cm,
  - H Field at center = 0.0 A/m,

- flux density at center = 0.0 T,
- 15.96 m of 14 AWG wire,
- aligned with horizontal vector of earth's magnetic field.

- **S1** Solenoid.
  - turns = 2703,
  - length = 0.76 m,
  - radius = 0.053 m,
  - Amperes = 3.0,
  - flux density = 1.35 $\times 10^{-2}$ T,
  - aligned with horizontal vector of earth's magnetic field and at vertical angle between 0° and 68°,
  - oriented with the negative side of the coil closest to the exposure.

- **S2** Solenoid.
  - turns = 2703,
  - length = 0.76 m,
  - radius = 0.053 m,
  - Amperes = 5.0,
  - flux density = 2.24$\times 10^{-2}$ T,
  - aligned with horizontal vector of earth's magnetic field and at vertical angle between 0° and 68°,
  - oriented with the negative side of the coil closest to the exposure.

- **E1** Electric Field.
  - 1.4×10^{5} V/m,
  - copper electrodes,
  - 3 cm separation,
  - in direction of orbital plane.

- **E2** Electric Field.
  - 2.4×10^{5} V/m,
  - copper electrodes,
  - 3 cm separation,
  - in direction of orbital plane.

3.4. Handling, development and processing

Film was handled only using vinyl gloves. Under recommended safelight illumination, the film was marked to indicate orientation and placed onto the exposure stage, normally in a north-south direction.

Film was then developed for 90 s immediately after exposure. Development was stopped with a water bath, normally fixed and dried. Using a Leitz Metalloplan microscope with a large stage, developed film was scanned at low magnification. At higher magnifications, selected tracks were measured using an eyepiece reticle calibrated with a stage micrometer and photographed using plano objectives and a calibrated Peltier-cooled 12 MP Jenoptik ProgRes C14 camera. Selected images were then aligned in mosaics, processed, measured and analyzed using ImageJ microscopy software and a set of custom track processing routines written in Python.

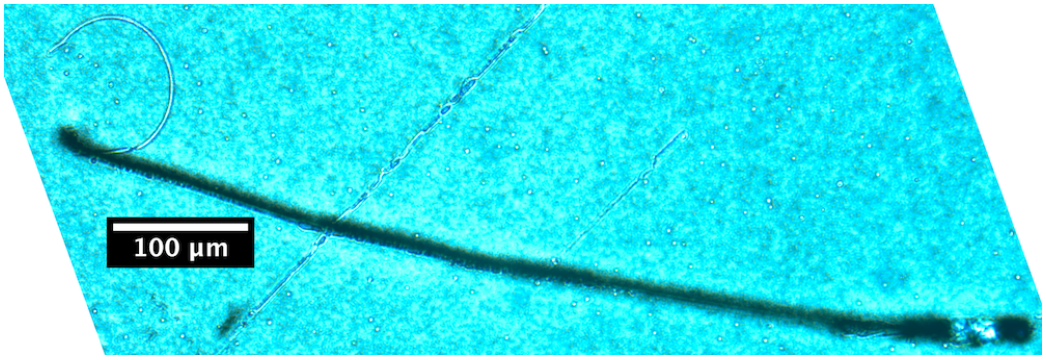

Figure 3. Track *lee2*, $n = 2.75$ showing ellipse at "end" of track. "Clear" ellipse emerges as if ejected from straight track with both clear and darkened components. Photographed at 160× using a Leitz PL 16× objective.

3.5. Observations

Experiments were performed with various electric and magnetic field configurations and various levels of light amplification of more than 750 exposures comprising a total photosensitive area of more than 2.85 m^2. No repeatable curvature resulting from the application of electric or magnetic fields was observed. It is possible that the conditions for electric or magnetic curvature of the particles was outside of the applied field strengths. It is also possible that applied fields played a role in the production of elliptic tracks. 102 of these tracks were candidates for elliptic curvature analysis. About 20% of the track candidates showed excellent unambiguous fits to ellipses.

The elliptic track type is a partial ellipse (ellipse segment) and can be described as a *comma* track. This type of curvature is observed either in standalone tracks or tracks indicating a particle decay event or a series of decays. If not a stand alone track, ellipses commonly appear at one end of a track (see Fig. 3) or as an intermediary component of a compound track, which may be a series of partial ellipses. Partial ellipses also commonly occur in pairs, multiples and swarms as do non-ellipse tracks (cf. [2] and see Section 9.1. Partial ellipses can be registered as black tracks or white tracks in the emulsion layer or clear tracks in the plastic base. On examination with 400× magnification, along with the darkening or bleaching of AgBr grains, many tracks show physical formation of voids, damage and/or ionization along $\sim 90\%$ of the track indicating particle traversal cutting a channel on the surface or directly through the AgBr/gelatin layer and/or plastic base of the film. Daviau et al. [7] using confocal and scanning electron microscopes, make the same point about particles cutting a groove or *tunneling* through layers of the emulsion and base. Due to the length and smooth curvature of the tracks, this indicates a particle detection with unusual characteristics and appears to rule out known charged particles.

In each case the elliptic tracks can be viewed as classical capture into and escape from a Kepler elliptic orbit in the plane of the film. In Fig. 5 (Bottom), the initial particle, P_1 decays into P_1' and P_2. P_2 is then captured into and subsequently escapes from an elliptic orbit.

In analogy with the gravitational case, we assume orbital capture of (charged) particle P_2 with mass m is possible due to a massive (charged) particle at the focus, F, of the ellipse in Fig. 5 (*Bottom*) with mass $M \gg m$ (and opposite charge). It is not clear why the particle escapes from the elliptic orbit.

Elliptic trajectories where $n > 3$ are observed to escape before aphelion. When $n < 3$, some ellipses are observed to continue on until almost complete.

3.6. Measurement

After creating a photomosaic of the track at high magnification, image processing is used to eradicate the background and x, y coordinates are extracted. Entry and exit points are determined by test hand-fitting followed by automated fitting using a progressive least-squares algorithm.

The procedure for measuring these tracks is as follows:

(1) Scan entire film for elliptic tracks using a microscope with 25× magnification.
(2) Locate elliptic track candidate and change to higher (≥160×) magnification.
(3) Locate, measure and record fiducial points near to track.
(4) Photograph the track in sections.
(5) Reconstruct track using mosaic (photomontage) software.
(6) Scale x, y track coordinates to x, y image coordinates.
(7) Threshold track image (image processing).
(8) Eradicate background (image processing).
(9) Get track center x, y coordinates (image processing).
(10) Determine ellipse entry and exit points.
(11) Fit ellipse to x, y coordinates.
(12) Report result as size of ellipse axes ± error. See Table 1.

3.7. Particle flux

Based on an average exposure and processing time of 180s with a detector square area of $\sim 3.8 \times 10^{-3}\text{m}^2$ and a nominal five total tracks per exposure, these particles have a differential flux of ~ 1.2 m^{-2} s^{-1} sr^{-1}. This compares with 1 m^{-2} s^{-1} sr^{-1} for 500 MeV electrons and 1.1 m^{-2} s^{-1} sr^{-1} for 500 MeV photons at sea level [15].

About 750 exposures with these parameters were carried out. Of these, 22 final ellipses were found, putting the total ellipse track flux at $\sim 1.8 \times 10^{-6}$ m^{-2} s^{-1}.

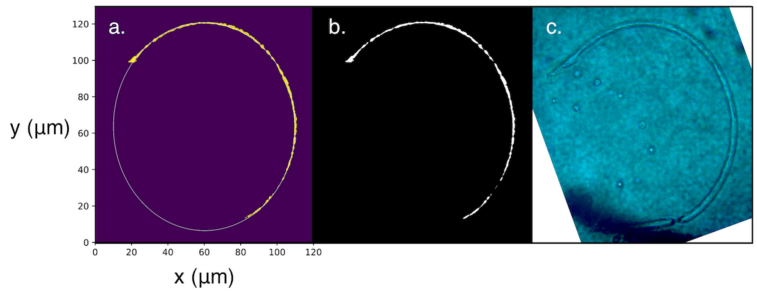

Figure 4. Track *lee2*, $n = 2.75$. (a) Ellipse fitted to track, semi-major axis size, $a = 56.9 \pm 13.0$ μm. (b) After processing and background eradication. (c) Photo at 1000× using Leitz PL 100× objective.

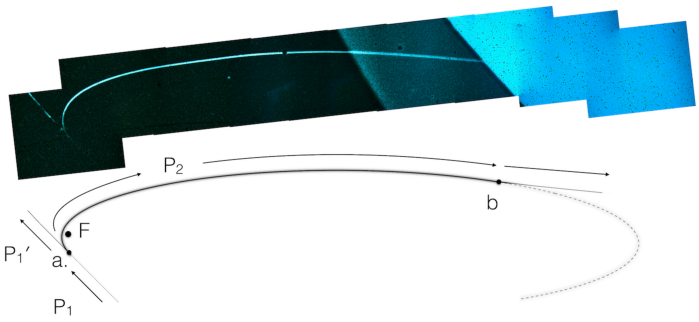

Figure 5. Track *me*, $n = 7$. *Top.* Semi-major axis size $a = 2391.6 \pm 16.1$ μm. Ten tile photomosaic at 160× using a Leitz PL 16× objective. See Fig. 6 for closeup of track. *Bottom.* Capture into and escape from an elliptic orbit. (1) Initial particle, P_1, trajectory. (2) *At point a*. Particle decays into P', continuing on initial trajectory and P_2, which is captured into an elliptic orbit. (3) *at point b*. Particle escapes from the elliptic orbit.

4. Framework for Analysis

4.1. $1/r^2$ force tracks in film

A $1/r^2$ central force and an orbiting particle are required to create an elliptic particle track in a nuclear track detector. The central force involved is active over a range from $\sim 2.54 \times 10^{-5}$ to 4.07×10^{-3} m. The strong force, weak force and gravity are negligible at these distances. Electrostatic central force is within the range with the largest known electron orbits of order $n \sim 1000$ in Rydberg atoms with radius 10^{-4} m [16], but is ruled out by the inability of tracks of known charged particles to register smooth curvature in emulsions. The remaining possibility is magnetostatic central force, i.e. a magnetic charge orbiting an opposite magnetic charge.

It is not possible for any *known* charged particle to record a significant part of an elliptic particle track or *any* track with appreciable smooth curvature with attainable magnetic fields in photographic emulsions. In this sense, these tracks are more like tracks in bubble chambers, that is, cutting through the relatively high density photographic emulsion like a hot knife through butter. So, we have the unusual situation of a particle traveling through a detector material as if that material had a much lower density than its known density and yet depositing very high levels of energy [2,4,5,7,10].

For known charged particles, scattering of the particle obscures any curvature and the most that can be expected of

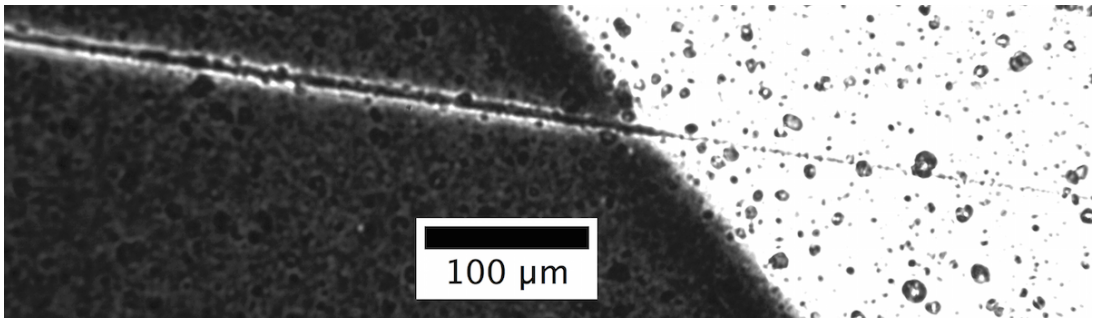

Figure 6. Detail of the $n = 7$ track showing track as blackened grains in dark area and as voids in plastic or gelatin in clear area. Note the *conventional* pattern similar to an ionizing particle in an emulsion (cf. periodic tracks in [2] and references therein).

Table 1. Ellipse semi-major, a, and semi-minor, b, axis measurements for each track along with associated quantum number, applied field setup, film type and associated applied field effect.

No.	track	$a(\mu$m)	$b(\mu$m)	n	Setup	Film	Effect
1	e2	4091.7±22.5	2241.3±22.5	8.00	trans BM	Rollei	Stark
2	be	4078.6±14.6	1996.0±14.6	8.00	E1+S1@26°	Arista	Zeeman
3	ode	4077.0±16.1	1129.4±16.1	8.00	no field	Arista	none
4	abt	4076.6±10.3	1053.6±10.3	8.00	E2+S1@68°	Arista	Zeeman
5	tlw	3141.0±30.5	1474.4±30.5	7.50	no field	Arista	none
6	me	2391.6±16.1	549.3±16.1	7.00	AH@0° DM	Arista	Stark
7	e1	1773.2±24.9	1100.5±24.9	6.50	trans BM	Rollei	Stark
8	ipe	1760.0±23.1	615.3±23.1	6.50	S1@68°	Arista	Stark
9	ego	908.9±21.8	505.8±21.8	5.50	S1@53°	Arista	Stark
10	ne	909.0±25.7	367.2±25.7	5.50	E1+YM	Rollei	Zeeman
11	bge	907.5±11.6	284.3±11.6	5.50	S1@53°	Arista	Stark
12	cav1	622.1±21.1	300.7±21.1	5.00	S1@32°	Arista	Stark
13	mct	619.9±16.2	192.7±16.2	5.00	DM+S1@68°	Arista	Stark
14	cce	621.1±7.3	173.8±7.3	5.00	S1@65°	Arista	Stark
15	edgee	254.2v7.4	104.8±7.4	4.00	S1@28°	Arista	Stark
16	sene	253.6±9.8	202.2±9.8	4.00	S1@65°	Arista	Stark
17	nne	149.8±13.1	83.0±13.1	3.50	S1@68°	Arista	Stark
18	ase	111.1±20.6	72.1±20.6	3.25	S1@53°	Arista	Stark
19	lee2	56.9±13.0	49.8±13.0	2.75	S1@68°	Arista	Stark
20	rse2	56.7±9.5	31.5 ±9.5	2.75	S1@65°	Arista	Stark
21	omse	38.1±6.2	36.0±6.2	2.50	S1@65°	Arista	Stark
22	avse2	25.6±6.4	15.9±6.4	2.25	S2@18°	Arista	Stark

Applied field legend: AH is the anti-Helmholtz, S1 the Solenoid – 1.35×10^{-2} T, S2 the Solenoid – 2.24×10^{-2} T, BM the Block Magnet – 1.26 T , DM the Disc Magnet – 1.32 T, YM the Yoked Magnet – 0.5 T, E1 the 1.4×10^5 V/m, and E2 is the 2.4×10^5 V/m. See Section 3.3 for applied field details.

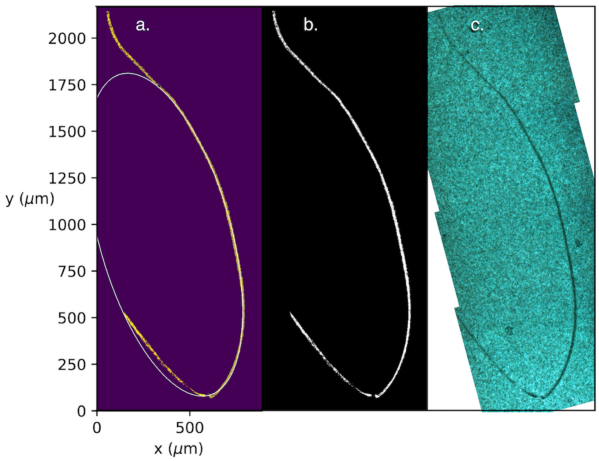

Figure 7. Track *ne*, $n = 5.5$. (a) Ellipse fitted to track, semi-major axis size, $a = 909.0 \pm 25.7$ μm. (b) Track after processing and background eradication. (c) Mosaic of track photographed with Leitz PL 16× objective.

measurements of curvature occurring entirely within photographic emulsions due to applied magnetic fields is to find the sign of charge [17].

Earlier studies [2,18] have detailed a catalog of tracks and associated properties such as have never been seen before in nuclear track studies. Properties include track lengths of more than 6.6 cm, lack of visible delta rays (indicating unconventional exposure), random motion trajectories (each containing dozens of extremely rare large-angle deflections) [3], smoothness and uniformity of track width over most of a given track, regular periodic structure [2] observation on many different film types and detector materials (see Section 2) correlated tracks and swarms [2], and bundles or tracks with internal structure [2].

An *idealized model* is created, analyzing geometry of tracks, neglecting scattering and energy loss of the particle as it travels through the detector material. Neglecting scattering could be considered as good approach based on the visual observation of smooth curved tracks in emulsions.

4.2. Geometric analysis

Ordinarily calibration with a known particle track type is done in nuclear emulsions for particle identification via particle energy loss. Since only geometric analysis of the tracks is being done in this case, this type of calibration is not required.

4.3. Magnetic monopoles

Dirac [19] showed that quantized magnetic charges (hereafter *monopoles*) could explain the quantization of electric charge and bring symmetry to Maxwell's equations. But the symmetry is not complete since the value of magnetic charge does not equal the value of electric charge.

The Dirac quantization condition [19],

$$g_{\mathrm{D}}^{(n)} = \frac{ecn}{2\alpha}\,, \quad n = (0, \pm 1, \pm 2, \pm 3, \ldots), \tag{1}$$

where $\alpha = k_e e^2/\hbar c$ and $k_e \equiv (4\pi\varepsilon_0)^{-1}$ with $n = 2$ gives

$$g = 2g_{\mathrm{D}} = \frac{ec}{\alpha}, \tag{2}$$

and is equivalent to the $n = 1$ *Schwinger Quantization* ($g = 2g_{\mathrm{D}}$) condition [20]. The Schwinger formulation removed Dirac's thin solenoid and gained *rotational* symmetry.

Using Eq. (1) with $n = 1$, the force between north and south magnetic poles is $\varepsilon_0\mu_0(g_{\mathrm{D}}/e)^2$ or 68.5^2 times stronger than the force between electric charges and using Eq. (2), the force difference or *ratio* between magnetic and electric charges is

$$\varepsilon_0\mu_0\left(\frac{g}{e}\right)^2 = \frac{n^2}{\alpha^2} \quad (g = 2g_{\mathrm{D}}), \tag{3}$$

or, with $n = 1$, $\alpha^{-2} = 137^2$.

If it exists, a classical monopole will move in an elliptic orbit around an oppositely charged pole at one focus and that pole should have a mass much greater than the orbiting pole.

Based on analogy with the electron and using $g = 2g_{\mathrm{D}}$, the magnetic coupling constant

$$\alpha_m = \alpha^{-1} = k_m\frac{g^2}{\hbar c} \quad (k_m \equiv \mu_0/4\pi), \tag{4}$$

where subscripts of m indicate magnetic, is just the reciprocal of the fine structure constant, α.

5. Particle Properties

In our idealized model, neglecting scattering and other perturbations to particle motion in the emulsion, fitted ellipses are compared to Bohr–Sommerfeld ellipses and various particle properties are computed.

The semi-major axes of the fitted ellipses, a_m, differ from the semi-major axes, $a_{\rm e}$, of corresponding Bohr–Sommerfeld ellipses for hydrogen by $\simeq 137^2 n^2$. Using $g = 2g_{\rm D}$,

$$137^2 n^2 \simeq \frac{a_m^{(n)}}{a_{\rm e}^{(n)}} = \frac{n^2}{\alpha^2}, \tag{5}$$

where subscripts of e stand for the electron and superscripts of (n) denote principal quantum numbers. Semi-major axis sizes and quantum numbers for the magnetic ellipses are determined using

$$a_m^{(n)} = a_{\rm e}^{(n)} \frac{n^2}{\alpha^2} \quad (\alpha = ec/g), \tag{6}$$

where α is the Schwinger quantization from (2). See Table 2. These are compared with the collection of fitted ellipses. In Fig. 1 measured ellipse sizes are shown to be quantized by half integer values from $n = 8$ to $n = 3.5$. Below $n = 3.5$, ellipse sizes appear to be quantized by quarter integer values.

5.1. Monopole mass

All orbits including the Bohr radius follow the same relation as Eq. (5), so that with $n = 1$,

$$\frac{a_{0m}}{a_{0\rm e}} = \frac{1}{\alpha^2}. \tag{7}$$

Using the formula for Bohr radius, $a_{0e} = \hbar/m_{\rm e}c\alpha$, the analogous $a_{0m} = \hbar/m_{\rm m}c\alpha_{\rm m}$ and Eq. (7), monopole mass can be written as

$$m_{\rm m} = \frac{m_{\rm e}\alpha^3}{\alpha_{\rm m}}\ , \tag{8}$$

and from Eq. (4), $\alpha_{\rm m} = \alpha^{-1}$, so

$$m_{\rm m} = m_{\rm e}\alpha^4 = 1.45 \times 10^{-3} \text{eV/c}^2, \tag{9}$$

which leads to the fine structure constant, $\alpha = (m_{\rm m}/m_{\rm e})^{1/4}$, as a mass ratio.

This value agrees with our independent prediction of monopole mass [21] based on $g = 2g_{\rm D}$ (see Section 6.3).

Table 2. Ellipse semi-major axis size, $a_{\rm m}$, energy, E, velocity, v and momentum, p for $n = \{1 - 8\}$. Mass, $m_{\rm m} = 1.45 \times 10^{-3}$ eV/c^2.

n	$a_{\rm m}$(m)	E(eV)	v(m/s)	p(eV/c)
1	9.93×10^{-07}	1.36×10^{01}	$4.11 \times 10^{+10}$	1.99×10^{-01}
2	1.59×10^{-05}	8.51×10^{-01}	$8.22 \times 10^{+10}$	2.48×10^{-02}
3	8.04×10^{-05}	1.68×10^{-01}	$1.23 \times 10^{+11}$	7.36×10^{-03}
4	2.54×10^{-04}	5.32×10^{-02}	$1.64 \times 10^{+11}$	3.11×10^{-03}
5	6.21×10^{-04}	2.18×10^{-02}	$2.05 \times 10^{+11}$	1.59×10^{-03}
6	1.29×10^{-03}	1.05×10^{-02}	$2.46 \times 10^{+11}$	9.20×10^{-04}
7	2.38×10^{-03}	5.67×10^{-03}	$2.88 \times 10^{+11}$	5.80×10^{-04}
8	4.07×10^{-03}	3.32×10^{-03}	$3.29 \times 10^{+11}$	3.88×10^{-04}

5.2. Monopole velocity

The ground state orbital velocity of the electron in hydrogen is $v_{0e} = k_e e^2/\hbar = c\alpha$ and the analogous ground state orbital velocity of the bound monopole

$$v_{0m} = k_m \frac{g^2}{\hbar} = c\alpha^{-1}, \tag{10}$$

where $v_{0m} > c$, once seen as required yet unphysical [22] is postulated as required, physical and aptly symmetric [21] with the electron, i.e. $v_{0e} = c\alpha$ below c and $v_{0m} = c\alpha^{-1}$ above c (see also Table 3).

5.3. Quantized energy levels

For the electron in hydrogen, energy is quantized according to

$$E_e^{(n)} = -k_e \frac{e^2}{2a_{0e}n^2} = \frac{E_{0e}}{n^2} = h\nu^{(n)}, \tag{11}$$

and for the bound monopole,

$$E_m^{(n)} = -k_m \frac{g^2}{2a_{0m}n^4} = \frac{E_{0m}}{n^4} = h\nu^{(n)} \ . \tag{12}$$

Note the n^{-2} vs. n^{-4} difference between the electron and monopole.

5.4. Kepler period

Using $g = 2g_D$, the Kepler period for an electron in hydrogen and the monopole in a magnetic hydrogen analog,

$$\tau_m^{(n)} = \frac{2\pi a_{0m} n^3}{v_{0m}} = \frac{2\pi a_{0e} n^3}{v_{0e}} = \tau_e^{(n)} \tag{13}$$

are equal.

6. A New Superluminal Transformation

6.1. Extended relativity

The concept of special relativity extended to superluminal velocities was perhaps best put by Corben [23] where our world is bifurcated at the speed of light with one sector (our regular world) moving at $v^2 < c^2$ and the other sector moving at $v^2 > c^2$ relative to us. The two sectors of the world are symmetric since what we observe as bradyons from the $v^2 < c^2$ sector will be observed as tachyons from the $v^2 > c^2$ sector and vice-versa. Observations by physicists in each world are defined as equivalent, but with rest frames at different relative velocities.

A cornerstone of the work done by Recami and others to extend special relativity to superluminal velocities is the superluminal Lorentz transformation or SLT [24,25] that connects observations made in a $v^2 > c^2$ frame with observations made in the $v^2 < c^2$ frame. A superluminal particle property observed by a subluminal observer needs to be transformed by an SLT to correspond to something that we would normally observe.

Using an SLT, length, time, momentum, energy and mass can all be transformed between $v^2 < c^2$ and $v^2 > c^2$ frames. Time-like vectors are transformed into space-like vectors and vice-versa. Velocity is transformed simply as $\beta \to 1/\beta$ where $\beta = v/c$.

In this framework, an electron from a $v^2 > c^2$ frame seen by an observer in a $v^2 < c^2$ frame is interpreted as an electron with superluminal Lorentz-transformed properties and *magnetic charge* of $g = -ec$ (bringing a more complete symmetry to Maxwell's equations). Slower-than-light monopoles are not predicted in this theory.

The collinear bi-dimensional (x, t) SLT works without problems, but, when extended to four dimensions (x, y, z, t), it leads to imaginary quantities for certain measurements of $v^2 > c^2$ objects and problems of how to interpret these physically. It is possible to use a six-dimensional space for the SLT, but there can be difficulties with the physical interpretation of two additional time dimensions.

If length is contracted using a collinear bi-dimensional transcendent [24] SLT along the *x*-axis and further (isotropic scale) contracted by an EM shift of α in accordance with the Schwinger quantization condition where $a_{\mathrm{m}}^{(n)} = x$, $a_{\mathrm{e}}^{(n)} = x'$, $b_{\mathrm{m}}^{(n)} = y$, $b_{\mathrm{e}}^{(n)} = y'$,

$$\begin{cases} a_{\mathrm{m}}^{(n)}(\alpha\gamma) = a_{\mathrm{e}}^{(n)} \\ b_{\mathrm{m}}^{(n)}(\alpha) = b_{\mathrm{e}}^{(n)} \end{cases} \qquad (\gamma = (\beta^2 - 1)^{-1/2}, \quad \beta > 1)\,. \tag{14}$$

As an example using theoretical $n = 8, \ell = 2$ ellipse data, ellipse size, orientation and eccentricity ($\mathcal{E} = 0.95 \rightarrow \mathcal{E}' = 0.99$) radically changes as a result of this *hybrid* SLT.

Using Recami's multidimensional approach, the SLT simply inverts the quadratic form sign [26] of an object and the shape of the monopole ellipse becomes

$$0 \geq -\frac{x^2}{a_{\mathrm{m}}^{(n)2}} + \frac{y^2}{b_{\mathrm{m}}^{(n)2}} \geq -1 \tag{15}$$

consisting of the area between an on-central-axis conic section,

$$\frac{y^2}{b_{\mathrm{m}}^{(n)2}} = \frac{x^2}{a_{\mathrm{m}}^{(n)2}}\,, \tag{16}$$

and a hyperbola,

$$\frac{y^2}{b_{\mathrm{m}}^{(n)2}} = \frac{x^2}{a_{\mathrm{m}}^{(n)2}} - 1, \tag{17}$$

greatly distorted from the original ellipse with eccentricity, $\mathcal{E}' > 1$, as shown in Fig. 8.

A real (vs. complex) SLT by Rajput et al. [27] results in an ellipse with the same semi-major axis size, same eccentricity,

The elliptic particle tracks we observe, (do they share geometrical properties of superluminal electrons?), do not share the same semi-major axis size as their (presumed) subluminal counterparts and do not appear to be distorted. That is, they appear to be scaled instead of stretched.

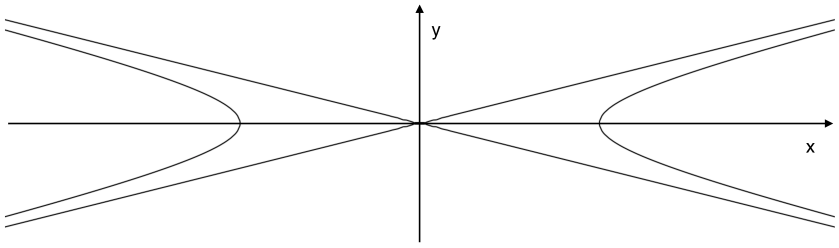

Figure 8. Recami type SLT of a theoretical $n = 8, \ell = 2$ monopole ellipse.

6.2. The Coulomb flip

If measured eccentricity corresponds to pure Bohr-Sommerfeld eccentricity, then, due to the α^{-2} size change, the transformation of ellipses in general needs to be an isotropic *scale* transformation instead of a translation along one axis.

The ratio of measured eccentricity, $\mathcal{E}_\mu$ to Bohr–Sommerfeld eccentricity, $\mathcal{E}_\tau$

$$\frac{\mathcal{E}_\mu}{\mathcal{E}_\tau} = \frac{\left(1 - b^2/a^2\right)^{1/2}}{n^{-1}\left(n^2 - \ell(\ell+1)\right)^{1/2}} \tag{18}$$

as a ratio of averages over the 22 track values, $\langle\mathcal{E}_\mu\rangle/\langle\mathcal{E}_\tau\rangle = 0.99$, and measured eccentricity corresponds well to Bohr–Sommerfeld electron orbit eccentricity. This implies that the superluminal transformation, for this restricted case of bound particles, should be a scale transformation.

The required transformation is just the force ratio, from Eq. (3), a scale ratio, dilatation (α^{-2}) or contraction (α^2) between magnetic and electric force strengths, which could be called the *Coulomb flip*.

The one-dimensional basis Coulomb flips from $\beta > 1$ to $\beta < 1$ are

$$\alpha_{\text{EM}}: \quad \alpha_{\text{m}}\left(\alpha^2\right) = \alpha_{\text{e}}, \tag{19a}$$

$$a_0: \quad a_{0\text{m}}\left(\alpha^2\right) = a_{0\text{e}}, \tag{19b}$$

$$v_0: \quad \alpha_{\text{m}} c\left(\alpha^2\right) = \alpha_{\text{e}} c, \tag{19c}$$

$$q^2: \quad k_{\text{m}} g^2\left(\alpha^2\right) = k_{\text{e}} e^2. \tag{19d}$$

Combining the basis transformations, Eqs. (19b)–(19d), and assuming $\hbar$ is Coulomb flip invariant, transformations for momentum, energy and mass are

$$\frac{\hbar}{a_{0\text{m}}} \xrightarrow[\alpha^2]{1} \frac{\hbar}{a_{0e}}, \quad p_{\text{m}}(\alpha^{-2}) = p_{\text{e}}, \tag{20a}$$

$$-\frac{k_{\text{m}} g^2}{2a_{0\text{m}}} \xrightarrow[\alpha^2]{\alpha^2} -\frac{k_{\text{e}} e^2}{2a_{0\text{e}}}, \quad E_{\text{m}}(\alpha^0) = E_{\text{e}}, \tag{20b}$$

$$\frac{\hbar}{a_{0\text{m}}\alpha_{\text{m}} c} \xrightarrow[\alpha^2\alpha^2]{1} \frac{\hbar}{a_{0\text{e}}\alpha_{\text{e}} c}, \quad m_{\text{m}}(\alpha^{-4}) = m_{\text{e}}, \tag{20c}$$

and the monopole and electron properties can be transformed into one another using Coulomb flips with $g = 2g_{\text{D}}$. In the ground state, time, in Eq. (13) and energy in Eq. (20b) remain invariant.

The 2-dimensional Coulomb flip scales the standard equation of the monopole ellipse (upper ellipse in Fig. 9), by the factor $(n^2\alpha^{-2})^2$,

$$\left(\frac{n^2}{\alpha^2}\right)^2 \left(\frac{x^2}{a_{\text{m}}^{(n)2}} + \frac{y^2}{b_{\text{m}}^{(n)2}}\right) = 1\,, \tag{21}$$

to the electron ellipse (lower ellipse in Fig. 9).

Since measurements made on the $v^2 < c^2$ and $v^2 > c^2$ sides of the world use (x, y, z) quantities all scaled by the same real factor, $(n^2\alpha^{-2})$, extending Eq. (21) to three dimensions, imaginary quantities do not enter the equations as they do in the determination of lengths orthogonal to the boost axis in the usual SLT. This scale transformation, resulting from interpretation of experiments, may, as a side-effect, solve the imaginary quantities problem [28] of SLTs.

The relativistic scale transformation could be termed a *Lorentz zoom* as opposed to a Lorentz boost. Relativistic scale transformations have been investigated by Nottale [29].

6.3. Equivalence of charges

Even though a superluminal particle's observed (by a subluminal observer) charge state is magnetic, it *should* possess exactly the same amount of charge in its own rest frame (the $v^2 < c^2$ frame) where the charge state is electric. This is to say that $v^2 > c^2$ electric charge is observed by normal subluminal observers to be magnetic charge and that subluminal magnetic charge does not exist [30,31].

As noted earlier, equivalence of charge along with considerations of special relativity prompted Recami et al. to set $g = -ec$ and abandon the Dirac quantization condition with respect to magnetic monopoles. In light of $g = 2g_{\mathrm{D}}$ it is possible to reconsider this issue.

The basis Coulomb flip for charge in Eq. (19d) shows that, after transformation, the magnetic charge is equivalent to the electric charge in a $v > c$ frame observed from a $v < c$ frame. Solving for g in (19d) with $k_{\mathrm{m}}/k_{\mathrm{e}} = 1/c^2$ yields $g = ec/\alpha$, which is the Schwinger quantization condition. So the Coulomb flip for charge is just the Schwinger quantization condition.

In an analysis of the Dirac quantization condition, Datta [22], found a new hierarchy of fundamental *monopole* lengths, $a_{0\mathrm{m}}, \lambda\!\!\!^{-}_{\mathrm{cm}}, r_{0\mathrm{m}}$, (Bohr radius, Compton wavelength and classical 'electron' radius) and pointed out that monopole bound states require superluminal ground state orbital velocities, but rejected the superluminal velocities as unphysical.

With *acceptance* of the required superluminal velocities and $g = 2g_{\mathrm{D}}$, a new hierarchy of fundamental lengths and corresponding velocities [21] (see Table 3) reproduces the extended relativity spacetime structure, but, in the restricted case of bound states, and due to the experimental result of Eq. (18), requires Coulomb flip scale transformations between subluminal and superluminal sides rather than SLTs.

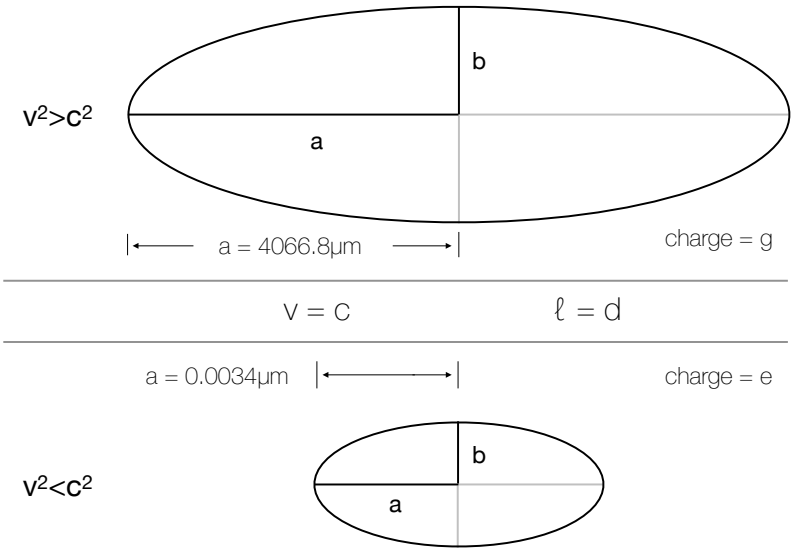

Figure 9. How a $v^2 < c^2$ observer sees a $v^2 < c^2$ electron orbit and an $n = 8$, $l = 2$ $v^2 > c^2$ monopole orbit. The $v^2 > c^2$ orbit is transformed to the $v^2 < c^2$ orbit using the 2-dimensional Coulomb flip Eq. (21) (not to scale).

Table 3. Velocity and length sequence alignment [21].

Velocity (m/s)			Length (m)		
			$\lambda_{ce}\alpha^{-5}$	$r_{0\mathrm{m}}$	1.86×10^{-2}
			$\lambda_{ce}\alpha^{-4}$	λ_{cm}	1.36×10^{-4}
4.11×10^{10}	$v_{0\mathrm{m}}$	$c\alpha^{-1}$	$\lambda_{ce}\alpha^{-3}$	$a_{0\mathrm{m}}$	9.93×10^{-7}
2.99×10^{8}	c	$c\alpha^{0}$	$\lambda_{ce}\alpha^{-2}$	d	7.25×10^{-9}
2.19×10^{6}	$v_{0\mathrm{e}}$	$c\alpha^{1}$	$\lambda_{ce}\alpha^{-1}$	$a_{0\mathrm{e}}$	5.29×10^{-11}
			$\lambda_{ce}\alpha^{0}$	λ_{ce}	3.86×10^{-13}
			$\lambda_{ce}\alpha^{1}$	$r_{0\mathrm{e}}$	2.82×10^{-15}

7. Applied Field Effects

As mentioned in Section 9, two main categories of tracks are distinguished, the predominant type and decays, which include the elliptic tracks. Effects of the electric and magnetic fields have not been observed for the predominant tracks. The central focus here is on the effect of the applied fields on the elliptic tracks.

In a similar manner to the way the electric charge is transformed to the magnetic charge and vice-versa using Coulomb flips (see Eq. (19d) and Section 6.3) applied electric and magnetic fields will also reverse roles.

If the applied electric field, now transformed to a magnetic field, is in a direction perpendicular to a superluminal electron orbiting a superluminal proton, it is possible that the Zeeman effect can occur. This is referred to as the *flipped* Zeeman effect. In the case of the Zeeman effect, both the semi-major and the semi-minor axes are affected by the magnetic field [32], so for tracks 2, 4 and 10 in Table 1, even though the field was not applied perpendicular to the orbit, but in the plane of the orbit, the principal quantum number *could* differ from the principal quantum number in the case of zero applied magnetic field and therefore the principal quantum number for these tracks may not be correct.

If the applied magnetic field, now transformed to an electric field, is in the direction of the plane of the orbit, it is possible that the Stark effect can occur. This is referred to as the flipped Stark effect. In the case of the Stark effect, only the semi-minor axis, related to changes in angular momentum, will be affected [33]. The principal quantum number will not be affected. Therefore the principal quantum numbers for tracks 6–9 and 11–22 in Table 1 should be correct, while the eccentricity and semi-minor axis size of these ellipses will be distorted with respect to the zero field case.

Tracks 3 and 5 had no applied electric or magnetic fields and so the principal quantum number should be correct as shown in Table 1.

So, the principal quantum number of tracks 3, 5–9 and 11–22 should be correct as shown in Table 1. Due to the flipped Zeeman effect, tracks 2, 4 and 10 *could* possess a different primary quantum number than that of an elliptic track without an applied magnetic field and as a result can be ignored in the analysis (although it does not change the main conclusions).

8. Track Formation Mechanism Inconsistencies

The mechanism of track formation is unknown and extremely unusual. We pointed out earlier [2] that the mechanism of track exposure is not clear. As mentioned in Section 2, tracks are observed on a number of materials besides the photographic emulsion (comprised of a dispersion of AgBr in gelatin on a polyester base), including Pd electrodes, MDS, (a semiconductor sandwich of Si, SiO_2 and Al), CR-39 (etched and unetched), PMMA, metal (Pb, W, and Al) foils, and glass. Commonly, the mechanism of track formation in photographic emulsions is ionization and to a lesser extent radiation [13]. The mechanism for (etchable) track formation in dielectrics and some semiconductors is ionization [34]. Etchable ion track formation in metals has been observed only using low-temperature GeV heavy ion

irradiation [35].

A number of contradictions exist in the observations of properties associated with track formation for the particles under consideration:

(1) Particle tracks in photographic emulsions with smooth curvature are not known to occur for any known particle, yet these are commonly observed for the tracks under consideration. Coulomb scattering should dominate the process of energy deposition while supressing any possibility of smooth curvature, and remain relatively constant along the track. Coulomb scattering in nuclear tracks has a characteristic look [3], which is not seen for these tracks. The only clear evidence of scattering that is seen is the large-scale scattering *in the observed capture process itself* (see Fig. 5), a relatively rare event.
(2) In the case of Bohr–Sommerfeld ellipses, we should see no energy loss from an elliptic orbit. By definition, these orbits have no dissipation and no energy loss. Furthermore, there is no known way to directly record an orbiting particle on a material detector, that is, where the particle would actually traverse the material. Yet, energy loss is large, in the elliptic tracks that fit with the Bohr–Sommerfeld model, as it is in all of these tracks.
(3) Analyses of energy deposition for these particles indicate very high energies (yet in the current study there is no known high energy source). In our 2013 study [2], we reported an average energy deposition estimate (linear stopping power) based on a grain density method developed by Katz [36] of ∼250 GeV/cm. Other studies used high-energy discharges, byproducts of discharges or laser illumination in electric and magnetic fields as sources of the tracks. Daviau et al. [7], based on comparison with alpha particle tracks, computed the energy necessary to carve the tracks in the MeV range. Adamenko and Vysotskii reported a value of 10^6 GeV/cm total energy release for the track type created in their study [10]. On the basis of the developed density of a track in the emulsion, assuming Coulomb braking, deposited energy was estimated at 700 MeV by Urutskoev and coworkers [4]. Skvortskov has estimated an energy loss of $\sim 10^4$ GeV based on the amount of material removed from tracks in metals [11].
(4) The "hairy rope" [36], track thickening toward the end of tracks, or other properties normally associated with ionization of high energy particles in emulsions is not seen.
(5) Monopoles should leave tracks similar to heavy nuclear fragments in emulsions [37], but these are not seen.
(6) Monopoles should exhibit constant track width over the entire track [38] and *thinning* [39,40] instead of thickening at the end of tracks. This *is* seen in our studies [2] (see also Fig. 10).
(7) Particles are either tunneling through AgBr/gelatin/plastic or digging deep trenches to make tracks [2,7].
(8) Adamenko and Vysotskii have forwarded a theory of track formation by nuclear reactions related to the passage of a magnetic monopole through a multilayer sandwich of Al, SiO_2 and Si because currently accepted theories of track formation apparently are not relevant.

The topic of mechanism of formation of these tracks is completely problematic. Our normal understanding of track formation *does not apply*. The entire question of energy deposition of these tracks is *completely unresolved*. With respect to how the tracks are formed, so far no scientific consensus has been reached.

If Coulomb scattering would be operative for formation of the elliptic tracks, it is reasonable to expect that the track geometry and the particle properties derived therefrom in this study would be different from the *actual* particle properties. But, it is *simply not possible* to achieve the level of Coulomb scattering normally associated with particle tracks in these tracks under consideration, which commonly exhibit smooth curvature in high density detectors like photographic emulsions because (for the most part) *scattering prohibits* [17] *measureable curvature* (and completely excludes *smooth* curvature).

In light of the preceding, any additional information on the behavior of these tracks occuring in materials is a welcome addition to the existing knowledge on the subject. The concept that the elliptic tracks could be formed in

approximate agreement with the presented idealized model cannot be evaluated based on an area of research that is inconsistent, *i.e.* the existing evidence for formation of these tracks in materials.

9. Discussion

These particles have been a mystery from the first known detection in 1979 (see [2]), using the photon amplification technique, to the experiments by Urutskoev and coworkers in 2000 and the various other experiments mentioned above in the ensuing years.

9.1. Earlier findings

The analyses of these experiments up to now have been based on certain observed particle properties such as the length of tracks, the curving of the tracks, the energy required to create a track in a certain material, etc.

Overall there has been agreement in the conjecture that these tracks are caused by monopoles [2,4–8,10,11,18,21,41,42]. Until now we have known about certain particle properties:

(1) *Periodicity*, visible in some (but not all) tracks, clearly indicates *regular oscillation* of the particle (or particle system) causing the track [2,4,5,7,9,11,18,41,42]. Orderly helical-like tracks as well as complex periodic tracks have been observed.
(2) *Penetration*, is apparent as many of the tracks possess very long track lengths, up to and more than $\sim$ 7 cm through photographic emulsions and other materials [2,4–7,41].
(3) *Random motion*, where the track undergoes many large-angle deflections like Brownian motion [2,7,18].
(4) *Correlation of tracks* [2,8,11,18,43] indicates a common origin of particles that are likely entangled. This also includes correlated random motion tracks and swarms [2].
(5) *Central force* evident from conformation of multiple correlated particle tracks [2,7,8,18,41]. Track geometry of correlated tracks indicates coordinated response arising from a central force.
(6) *Tracks in various materials*, *i.e.* plastic, gelatin, metals, semiconductors and glass [2,9–11] gives information about the energy of these particles.
(7) *Large angles of curvature* or abrupt changes of directions of tracks [2,8,41] may give information about the mass, charge and decay of particles.
(8) *White tracks* in addition to black tracks indicate a tearing down of the latent image. These tracks can only be a result of exposure after or during the supplemental photon exposure, thus constraining the exposure time to the elapsed time after photon exposure till start of development. These tracks have only been observed in Fredericks [2]. The AgBr emulsion, re-zeroed at a higher level of sensitivity, able to respond in two directions, may be exactly the type of detector Terletskii [44] suggested as necessary to detect a negative energy particle.

Skvortsov has made mass estimates in a range of $\sim 10^{-3}$eV/c^2 [45] and $\sim 10^{-2}$eV/c^2 [11], based on the peak-to-peak amplitude of a periodic (clear) track in CR-39 (etched for 20 min. in an alkali solution). Mass shown in Eq. (9), 1.45×10^{-3} eV/c^2, is within this range.

9.2. New findings

The series of experiments culminating in detection of elliptic curvature of new tracks in emulsions and the subsequent analysis brings a new critical set of particle properties:

(1) Tracks show decay events, some of which are elliptic tracks emitted from a central track (see Fig. 10), showing two distinct track types, i.e. decays, which include elliptic tracks, and predominant tracks, which include everything else.

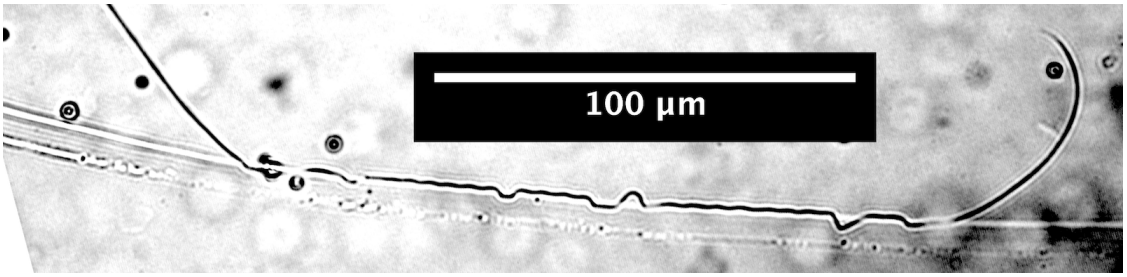

Figure 10. Track *rse2*, $n = 2.75$ showing elliptic track decay event. Photo at 400× using Leitz PL 40× objective. Notice also constant track width over the entire range [38] and track thinning [39,40] at the end of the track.

(2) Exposures with and without applied electric and/or magnetic fields show nearly identical results in terms of overall track curvature. Predominant tracks are observed as curving one way and then the other or as long straight tracks. These particles (or composite particle systems) appear to behave as if neutral or the applied electric and magnetic fields are not in the right range to repeatably affect the particles.
(3) Partial elliptic tracks show quantized semi-major axis sizes $a_{\mathrm{m}}^{(n)}, n^2\alpha^{-2}$ larger than Bohr–Sommerfeld hydrogen with quantized energy levels $E^{(n)} = h\nu^{(n)}$.
(4) Ground state velocity based on the elliptic tracks and analogy with the electron is α^{-2} greater than the electron ground state velocity in hydrogen, and therefore superluminal.
(5) Coulomb flips of the new particle momentum, energy and mass match with a superluminal electron with $m_0 = 5.11 \times 10^5$ eV/c^2.
(6) The Coulomb flip of Eq. (19a) constitutes a single EM coupling constant, α_{EM}, which inverts with velocity

$$\alpha_{EM} = \begin{cases} \alpha & \text{if} \quad \beta < 1 \\ \alpha^{-1} & \text{if} \quad \beta > 1 \end{cases}. \tag{22}$$

(7) Mass, m_{m}, based on the elliptic tracks and analogy with the electron, which is the relativistic mass of the electron, is $m_{\mathrm{e}}\alpha^4$ smaller than the electron rest mass, giving a mass ratio equal to the fine structure constant from Eq. (9), $\alpha = (m_{\mathrm{m}}/m_{\mathrm{e}})^{1/4}$.
(8) Charge quantization based on special relativity, *i.e* Dirac's cause of quantization is the presence of magnetic charge, which is satisfied by the corresponding superluminal charge state of the electron, which to the subluminal electron is indistinguishable from magnetic charge.

The key point is item 5 that, using the Coulomb flip, the particle tracks correspond directly to the geometry of electrons from a superluminal frame.

Application of electric and magnetic fields during exposures that create these tracks shows no hard evidence of affecting predominant track curvature. This seems to be contradictory since only charged particles should be recorded and, if recorded, should respond to magnetic and/or electric fields. However, the particle (or composite particle system) behaves as if neutral. Decay events, where particle tracks emerge from a main track, however, do exhibit repeatable curvature, may be susceptible to EM fields, and, as mentioned in item 1, show two specific particle types. Note that Daviau and coworkers [7] earlier referred to this decay as *branching*.

According to the Heisenberg uncertainty principle, our elliptic orbits should be smeared or diffuse, not sharp tracks. This question is beyond the current scope but the subject of an upcoming investigation.

9.3. Theoretical approaches

Georges Lochak [41,42] has investigated these tracks and has looked specifically at the tracks produced in experiments by Urutskoev et al. [4,5], Ivoilov [8,46], Daviau et al. [7], Bardout et al. [47] and Priem et al. [6,48] and suggests that these are light leptonic monopoles that are magnetically excited neutrinos. Lochak believes that these particles are linked to composite particles following de Broglie's theory of light [42]. Writing the equations for a nonlinear massive monopole, Lochak shows (as an aside) how tachyon states appear and that these states exist also for the nonlinear neutrino. Lochak cites Recami and Mignani in relation to this hypothesis. He also believes, based on work by Urutskoev and coworkers and Ivoilov, that these particles are extremely numerous.

Independent of the particle track data, Stumpf [49] elaborates on Lochak's ideas of the light leptonic magnetic monopole and composite particles on the basis of Urutskoev et al.'s [4,5] use of discharges in water as the source of low-energy nuclear reactions. Stumpf is in agreement with Lochak regarding the magnetically excited neutrino hypothesis and looks to extend the standard model to include these types of particles.

In the track images where a decay is taking place, i.e. a particle is seen flying off at an angle to a main trajectory, one can assert the idea of two or more particles traveling together, but then separating when a certain energetic conditions are met. The composite particle system concept may well fit with the physical evidence seen in these types of tracks.

9.4. The Coulomb lens

The Coulomb flip likely provides a superluminal transformation without the introduction of imaginary quantities, allowing switching between electric and magnetic worlds and transforming all of the ellipses in the study from monopole to electron orbits. This would mean that superluminal objects could provide a portal of magnification, analogous to gravitational lensing, into our own world, that electron orbits could be examined in a way never before available, like looking at partial atomic electron orbits using the $\alpha^{-2}\times$ ($\sim 1.88 \times 10^4\times$) magnification using what might be called a Coulomb lens.

10. Concluding Remarks

It should not be possible for any *known* particle to create the type of smooth elliptic tracks in photographic emulsion shown in Figs. 2,3,5,6, and 10 and the ranges of possible central forces suggests the elimination of all but magnetic force as the cause of these tracks. Using an idealized analysis based on analogy between the electron and magnetic monopole and the track geometry, a modification to extended relativity is developed, resulting in the Coulomb flip to transform between $v^2 < c^2$ and $v^2 > c^2$ frames.

Using a geometrical analysis and analogy with the electron, these particles are shown to possess a (relativistic) mass of 1.45×10^{-3}eV/c^2 and a superluminal velocity. A related yet independent analysis [21] based on the Schwinger quantization condition shows that due to the size of the orbits these particles must possess superluminal velocities and a mass of 1.45×10^{-3}eV/c^2. Using a new extended relativity model, the experimental results appear to be consistent with the detection of superluminal electrons with $m_0 = 5.11 \times 10^5$eV/c^2.

The idealized model adds new information to the overall understanding of these new types of particle tracks. Inconsistencies in the understanding of track formation mechanisms for these tracks precludes the application of any error arising from track formation that might affect the idealized model since one cannot say exactly what that error is. Additional work needs to be done to determine track formation mechanisms and particle interactions so as to understand what error should be taken into consideration in the geometric analysis of these tracks.

A new model builds upon The Dirac/Schwinger quantization condition, Recami and Mignani's extended theory of relativity and Coulomb's law to bring a simple superluminal scale transformation presumably without imaginary quantities in the Coulomb flip. Distortion observed by subluminal observers may well be that of a uniform scale change

and not a shape change as a result of a translation. Detection of superluminal objects may open a path to substantial magnification of submicroscopic objects analogous to, but with a much greater magnification than, gravitational lensing for astronomical objects.

Acknowledgments

The author thanks Jacques Consiglio for essential help and stimulating discussions and is also grateful to Moses Fayngold, Giovanni Modanese and Leonid Urutskoev for important suggestions and interest in this work.

References

[1] L. Epele, H. Fanchiotti, C. Garcia Canal and V. Vento, *Euro. Phys. J.* C **56** (2008) 87.
[2] K.A. Fredericks, *Eng. Phys*. **6** (2013) 15.
[3] C.F. Powell, *The Study of Elementary Particles by the Photographic Method,* Pergamon, London, 1959; W.H. Barkas, *Nuclear Research Emulsions,* Vol. 1: *Techniques and Theory,* Academic Press, New York, 1963; W.H. Barkas*, Nuclear Research Emulsions,* Vol. 2*: Particle Behavior and Emulsion Applications*, Academic Press, New York, 1973.
[4] L.I. Urutskoev, V.I. Liksonov and V.G. Tsinoev, *Ann. Fond. L. de Broglie* **27** (2002) 701, arXiv:physics/0101089.
[5] L.I. Urutskoev, *Ann. Fond. L. de Broglie* **29** (2004) 1149.
[6] D. Priem, C. Daviau and G. Racineux, *Ann. Fond. L. de Broglie* **34** (2009) 103.
[7] C. Daviau, D. Fargue, D. Priem and G. Racineux, *Ann. Fond. L. de Broglie* 38 (2013) 139.
[8] N.G. Ivoilov, *Ann. Fond. L. de Broglie* **31** (2006) 115.
[9] B. Rodionov and I. Savvatimova, in *Proc. 12th Int. Conf. on Cold Fusion*, A. Takahashi, K. Ota and Y. Iwamura (Eds.), World Scientific, Singapore, 2005, Chap. 44, pp. 421–429; I. Savvatimova and J. Dash, in *The 9th Int. Conf. on Cold Fusion, Condensed Matter Nuclear Science*. 2002. Tsinghua Univ., Beijing, China, Z.Z. Li (Ed.), Tsinghua Univ. Press, 2002.
[10] S. V. Adamenko and V. I. Vysotskii, in *Proc. 14th Int. Conf. on Condensed Matter Nuclear Science on Cold Fusion (ICCF-14)* 10–15 August 2008, Washington DC, D.J. Nagel and M.E. Melich (Eds.), New Energy Foundation Inc., 2008, p. 484; S.V. Adamenko and V.I. Vysotskii, *Ann. Fond. L. de Broglie* **33** (2008) 13.
[11] V.A. Skvortsov and N.I. Vogel, in Exotic nuclei: EXON-2014, *Proc. of Int. Symposium*, Y. Penionzhkevich and Y. Sobolev (Eds.), World Scientific, Singapore, 2015, pp. 457–463.
[12] H.D. Ables, *AAS Photo-Bull*. **3** (1971) 18T. A. Babcock, *AAS Photo-Bull*. **13** (1976) 6.
[13] T.H. James, *The Theory of the Photographic Process*, Fourth Edn. Macmillan, New York, 1977.
[14] R.P. Czwakiel and E.C. Scott, *Proc. SPIE* **0058** (1975) 192.
[15] G. Kaye, T. Laby and N.P.L.G. Britain, *Tables of Physical & Chemical Constants,* 16th Edn. 1995, 2.7.7 Cosmic Rays, Kaye & Laby Online. Version 1.0 (2005),National Physical Laboratory, 2005.
[16] V. Lebedev and I. Beigman, in *Physics of Highly Excited Atoms and Ions*, Springer, Berlin, Heidelberg, 1998, pp. 1–9.
[17] C. Dilworth, S. Goldsack, Y. Goldschmidt-Clermont and F. Levy, *Philos. Mag*. **41** (1950) 1032, I. Barbour, *Phys. Rev.* **78** (1950) 518, M. Merlin, *Nuovo Cimento* **11** (1954) 218.
[18] K.A. Fredericks, *J. Condensed Matter Nucl. Sci.* **15** (2015) 203.
[19] P.A.M. Dirac, *Proc. Royal Soc*. A **133** (1931) 60, P.A.M. Dirac, *Phys. Rev*. **74** (1948) 817.
[20] J. Schwinger, *Phys. Rev*. **144** (1966) 1087.
[21] K.A. Fredericks, *Phys. Essays* **30** (2017) 269.
[22] T. Datta, *Lett. Nuovo Cimento* **37** (1983) 51.
[23] H.C. Corben, *Int. J. Theoret. Phys*. **15** (1976) 703.
[24] E. Recami and R. Mignani, *Nuovo Cimento* **4** (1974) 209, E. Recami, *Nuovo Cimento* **9** (1986) 1.
[25] L. Parker, *Phys. Rev*. **188** (1969) 2287.
[26] A. Barut, G. Maccarrone and E. Recami, *Nuovo Cimento* A **71** (1982) 509.
[27] B.S. Rajput, P. Joshi and O.P.S. Negi, *Lett. Nuovo Cimento* **35** (1982) 147.
[28] H.C. Corben, *Lett. Nuovo Cimento* **11** (1974) 533.

[29] L. Nottale, *Found. Sci*. **15** (2010) 101.
[30] R. Mignani and E. Recami, *Lett. Nuovo Cimento* **9** (1974) 367.
[31] E. Recami and R. Mignani, *Lett. Nuovo Cimento* **9** (1974) 479.
[32] W.-D.R. Stein, *J. Russ. Laser Res.* **34** (2013) 553.
[33] J. C. Solem, *Am. J. Phys*. **55** (1987) 906, https://doi.org/10.1119/1.14951.
[34] R. Fleischer, P. Price and R. Walker, *Nuclear Tracks in Solids: Principles and AppliCations,* University of California Press, USA, 1975.
[35] A. Barbu, H. Dammak, A. Dunlop and D. Lesueur, *MRS Bull*. **20** (1995) 29–34.
[36] R. Katz, *Nucl. Instrum. Meth*. B **40–41** (1989) 1271.
[37] E. Bauer, *Math. Proc. Cambridge* **47** (1951) 777–789.
[38] R. Katz and J.J. Butts, *Phys. Rev*. **137** B (1965) 198.
[39] R. Katz and D.R. Parnell, *Phys. Rev*. **116** (1959) 236.
[40] H.J.D. Cole, *Math. Proc. Cambridge* **47** (1951) 196–206.
[41] G. Lochak, *Z. Naturforsch.* A **62** (2007) 231, arXiv:0801.2752 (quant-ph) .
[42] G. Lochak, in *The Leptonic Magnetic Monopole Theory and Experiments, Advances in Imaging and Electron Physics*, Vol. 189, P.W. Hawkes (Ed.), Elsevier, Amsterdam, 2015, pp. 1–172.
[43] V.A. Skvortsov and N.I. Vogel, in Exotic nuclei: EXON-2014, *Proc. Int. Symposium*, Y. Penionzhkevich and Y. Sobolev (Eds.), World Scientific, Singapore, 2015, pp. 465–470.
[44] Y.P. Terletskii, *Paradoxes in the Theory of Relativity,* Plenum, New York, 1968, pp. 102–104.
[45] V.A. Skvortsov and N.I. Vogel, in *Proc. 29th EPS Conference on Plasma Phys.,* ECA **26** B (2002) D-5.013.
[46] N.G. Ivoilov and L.I. Urutskoev, *Ann. Fond. L. de Broglie* **29** (2004) 1177.
[47] G. Bardout, G.Lochak and D. Fargueb, *Ann. Fond. L. de Broglie* **32** (2007) 551.
[48] D. Priem, G. Racineux, G. Lochak, C. Daviau, D. Fargue, M. Karatchentcheff and H. Lehn, *Ann. Fond. L. de Broglie* **33** (2008) 129.
[49] H. Stumpf, in The leptonic magnetic monopole theory and experiments, *Advances in Imaging and Electron Physics*, Vol. 189, P.W. Hawkes (Ed.), Elsevier, Amsterdam, 2015, pp. 173–314.